JOURNAL OF GUIDANCE, CONTROL, AND DYNAMICS
Vol. 16, No. 1, January-February 1993

Experiments in Multivariable Adaptive Control of a Large Flexible Structure

C.-H. C. Ih,* D. S. Bayard,* A. Ahmed,† and S. J. Wang*
Jet Propulsion Laboratory, California Institute of Technology, Pasadena, California 91109

A six-input/six-output multivariable adaptive controller is used to control a large three-dimensional flexible structure experiment. For this purpose, the Jet Propulsion Laboratory Large Spacecraft Control Laboratory antenna-like experiment structure is used, with instrumentation distributed on both the hub and the ribs. This represents a significant increase in complexity relative to earlier adaptive control experiments performed on the same structure using a two-input/two-output setup with instrumentation on the hub alone [Ih, C.-H. C., Bayard, D. S., Wang, S. J., and Eldred, D. B., "Adaptive Control Experiment with a Large Flexible Structure," Proceedings of the AIAA Guidance, Navigation, and Control Conference (Minneapolis, MN), AIAA, Washington, DC, Aug. 1988 (AIAA Paper 88-4153)]. The increase in instrumentation significantly increases spatial controllability and excitation and control of a much larger set of modes. This paper documents multivariable adaptive control experiments on this structural configuration and discusses many of the associated design and implementation issues required for successful operation.

I. Introduction

DEVELOPMENTAL research on the application of adaptive control to large flexible structures has been evolving in recent years. In spite of such efforts, experimental work in this area remains somewhat limited, especially in the multi-input/multi-output setting. The present effort will demonstrate multivariable adaptive control for the Jet Propulsion Laboratory (JPL) Large Spacecraft Control Laboratory (LSCL) three-dimensional large flexible structure experiment.[2] This facility has been specifically designed for emulating the behavior of large flexible space structures operating in an on-orbit environment.

Generally speaking, the adaptive algorithms which have been implemented experimentally to date fall in either of two categories: indirect and direct adaptive control. Indirect algorithms have the advantage of being applicable to nonminimum phase plants but have the disadvantage of requiring parameter convergence, and hence require persistence of excitation. The persistence of excitation condition requires one to add a "dither" to the control signal that improves learning but upsets the attainable closed-loop control performance.

Parameter convergence may itself be difficult to achieve because of the high-order dynamics and large number of parameters typically associated with the large flexible structures application. In contrast, direct adaptive control techniques do not require persistence of excitation, but have the disadvantage of being applicable to only minimum phase plants. In a structural control context, this means that direct adaptive control algorithms are generally restricted to structures with collocated actuators and sensors.

Indirect adaptive techniques which were demonstrated experimentally include that of Eldred and Schaechter on the JPL Flexible Beam Facility[3] using an extended Kalman filter followed by a discrete linear quadratic (LQ) control design; Sundararajan et al. on the NASA Langley free-free beam and two-dimensional flexible grid[4] using lattice filter identification followed by a modal control design; the work of Sidman on adaptive pole-placement for the Stanford four disk system;[5] and Rovner and Franklin using a modified self-tuning LQ design[6] on a flexible one-link robotic manipulator at Stanford.

Direct adaptive techniques were demonstrated experimentally on the JPL LSCL experiment facility by Ih et al.[1] using a collocated two-input/two-output adaptive control design. The adaptive algorithm was based on an approach put forth in Bayard et al.[7] that modifies and extends an earlier algorithm due to Sobel et al.[10] The results were encouraging, providing stable transient regulation with significant improvement over the open-loop performance. However, by restricting instrumentation to the hub, the dynamics of the study were intentionally limited to the "boom-dish" modes, i.e., the subset of modes observable and controllable from the hub.

In the present study, the instrumentation is mounted on the ribs as well as the hub of the structure. With this configuration, the rich dynamics of the pure "dish modes" become observable and controllable, augmenting the boom-dish modes just described. With this augmentation, the dynamics of the system model become significantly richer, and control authority is extended over a larger domain of the structure. Multivariable adaptive control is demonstrated for this complex configuration, and many of the associated design and implementation issues required for successful operation are discussed.

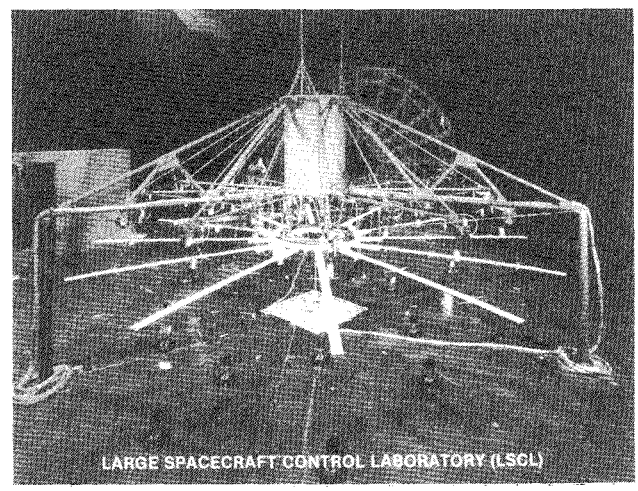

Fig. 1 Experiment structure.

Received Sept. 8, 1989; revision received Dec. 2, 1991; accepted for publication Feb. 24, 1992.

*Research Scientist, Guidance and Control Section. Member AIAA.
†Research Scientist,Guidance and Control Section.

II. Experiment Structure and Configuration

A brief overview of the facility is provided here. A more detailed description can be found in Refs. 1 and 2.

The physical experiment and supporting backup structure are depicted in Fig. 1. The structure consists of a central circular hub connected to 12 ribs and a flexible boom that is attached to the hub and hangs below it. The ribs are coupled together by two rings of pretensioned wires that provide coupling of motion in the circumferential direction. These coupling wires complicate the dynamics in order to emulate the effect of a simple mesh. The diameter of the structure is 18.5 ft and the ribs are extremely flexible. The large size and great flexibility are necessary to achieve the low modal frequencies representative of large space structures.

A bird's-eye view of the structure and associated instrumentation is depicted in Fig. 2. For the present multivariable adaptive control experiment, the following collocated actuator/sensor pairs will be used:

Hub
HA1/HS10
HA10/HS1

Ribs
RA1/RS1
RA4/RS4
RA7/RS7
RA10/RS10

The hub torquers HAi, $i = 1, 2$, are actually linear force actuators that provide torque to the hub by pushing at its outer circumference. The torque provided is equal to the force times the lever arm about the axis of rotation. The hub sensors HSi, $i = 1, 2$, measure angular position by rotary variable differential transformers (RVDTs) mounted directly on the gimbal bearings. Note that each hub sensor measures the structural response to the actuator mounted orthogonal to it. Hence, although the actuator/sensor pairs HA1/HS1 and HA10/HS10 are physically collocated, it is HA1/HS10 and HA10/HS1 that are collocated in the sense of "dual" variables in a dynamical description.

The rib root actuators RAi, $i = 1, 4, 7$, and 10, are solenoid-based designs that provide the desired torque by reacting against a mount that is rigidly attached to the hub. These actuators are collocated with the four rib root sensors RSi, $i = 1, 4, 7$, and 10, which measure angular rib displacement using linear variable differential transformers (LVDTs).

The instrumentation just outlined represents a considerable upgrade relative to the earlier control experiments[1] that utilized only the hub actuation/sensing pairs (i.e., HA1/HS10 and HA10/HS1). The instrumentation on the ribs extends controllability to a much richer set of modal dynamics. This will be described in more detail below.

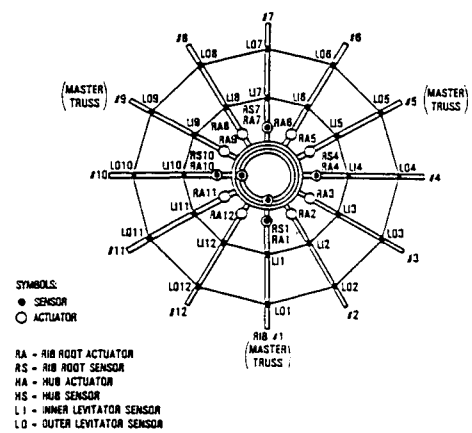

Fig. 2 Bird's-eye view of structure and instrumentation.

III. Dynamic Model

The symmetry of the structure makes it possible to separate variables and write the dependence of the system mode shapes on a circular wave number k. Mode shapes of the structure can be conveniently grouped according to their circular wave number, which can range from $k = 0$ to $k = 6$. In particular, it is convenient to make the following definitions:

$k = 1$: "boom-dish" modes

$k = 0, 2, 3, 4, 5, 6$: "dish" modes

Modes with $k = 1$ are asymmetric about the hub and can be observed and controlled using hub instrumentation. These are denoted as "boom-dish" modes because the mode shapes involve the boom and dish moving together. In contrast, modes with $k = 0, 2, 3, 4, 5$, and 6 are symmetric about the hub in the sense that all reaction forces on the hub caused by the ribs exactly cancel out. These are denoted as "dish modes," since the hub and boom do not participate in the modal motion. The lowest modal frequencies of the structure, as determined by a finite element analysis, are listed in Table 1.

An important property of the dish modes is that they are all uncontrollable and unobservable from the hub. Thus it is possible, by using only the hub actuators and sensors, to excite and control only the boom-dish modes. Since these modes constitute a small subset of all of the system modes, the resulting control problem is much more tractable. The adaptive control experiments described in the earlier paper[1] control only the boom-dish modes; the present paper will tackle the more difficult problem of adaptively controlling the dish modes as well.

IV. Adaptive Control Algorithm

The adaptive control algorithm is described briefly in this section. A more detailed discussion can be found in Ref. 1 and the stability proof can be found in Ref. 7.

The flexible structure dynamics are conveniently written in state-space form as

$$\dot{x}_p(t) = A_p x_p(t) + B_p u_p(t) \tag{1}$$

$$y_p(t) = C_p x_p(t) \tag{2}$$

where $x_p \in R^{N_p}$, $u_p \in R^M$, $y_p \in R^M$; and A_p, B_p, and C_p are of appropriate dimensions. It is assumed that (A_p, B_p) is controllable and (A_p, C_p) is observable. Physically, the output y_p is a weighted sum of position and rate measurements, where the position-to-rate ratio is given by α, i.e.,

$$y_p = \alpha y_{\text{pos}} + y_{\text{rate}} \tag{3}$$

Of course, direct rate measurements y_{rate} are not available on the facility. However, we will proceed with the algorithm assuming they are, and in practice, estimate rate from position measurements using a Kalman filter. This is an implementation issue that will be discussed in Sec. V.

A stable reference model which specifies the desired performance of the plant is described by the following state-space representation:

$$\dot{x}_m(t) = A_m x_m(t) + B_m u_m(t) \tag{4}$$

$$y_m(t) = C_m x_m(t) \tag{5}$$

where $x_m \in R^{N_m}$, $u_m \in R^M$, $y_p \in R^M$; A_m, B_m, and C_m are of appropriate dimensions; and u_m is assumed to be a step function.

It is noted that the reference model order can be smaller than the plant order. Define the output error between the plant and the model as

$$e_y(t) = y_m(t) - y_p(t) \tag{6}$$

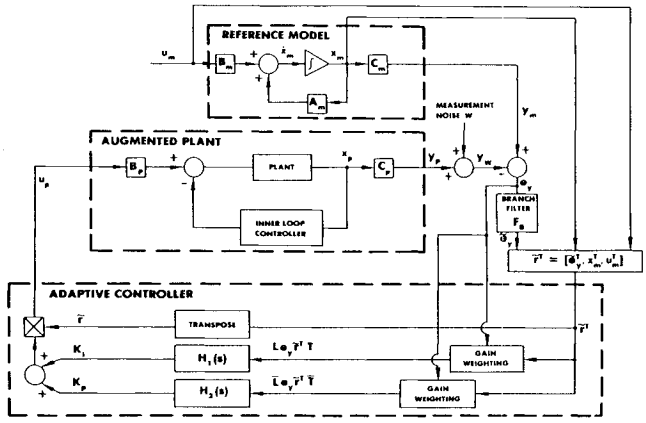

Fig. 3 Adaptive control system block diagram.

It is desired to adaptively control the plant so that it tracks the model asymptotically at the output.

$$\lim_{t\to\infty} e_y(t) = 0$$

The adaptive control is written as

$$u_p = K\tilde{r} \tag{7}$$

where

$$\tilde{r}^T = [\tilde{e}_y^T, x_m^T, u_m^T]^T \tag{8}$$

$$K(t) = [K_e, K_x, K_u] \tag{9}$$

and $\tilde{e}_y$ is the output of the branch filter F_B designed to suppress output noise.

$$\tilde{e}_y = F_B(e_y) \tag{10}$$

The adaptive gain K is chosen as the sum of a proportional and integral component:

$$K(t) = K_p(t) + K_I(t) \tag{11}$$

where K_I and K_p are each outputs of linear systems:

$$K_I = C_1 X_1 \tag{12}$$

$$\dot{X}_1 = A_1 X_1 + B_1 L e_y \tilde{r}^T T \tag{13}$$

$$K_p = C_2 X_2 \tag{14}$$

$$\dot{X}_2 = A_2 X_2 + B_2 \bar{L} e_y \tilde{r}^T \bar{T} \tag{15}$$

Here, X_1, $X_2 \in R^{\eta_2 \times (2M+N_m)}$ are *matrix* states. Sufficient conditions for global stability are derived in Ref. 7 and are summarized as follows:

1) $T, \bar{T}, L, \bar{L} > 0$.

2) There exists a $P = P^T > 0$ and $Q = Q^T > 0$ such that $PB_p = C_p^T$ and $PA_p + A_p^T P = -Q$.

3) H_1 and H_2 are strictly positive real (SPR), where $H_1(s) = C_1(sI - A_1)^{-1}B_1 L$ and $H_2(s) = C_2(sI - A_2)^{-1}B_2\bar{L}$.

4) Rank $\{[C_1 : C_2]\} = M$.

5) $F_B(\cdot)$ is any bounded input/bounded output (BIBO) stable linear or nonlinear filter.

Condition 2 is equivalent to the assumption that the open-loop plant transfer function matrix

$$Z(s) = C_p(sI - A_p)^{-1}B_p \tag{16}$$

is SPR. For a collocated structure having small but nonzero intrinsic damping, this condition can always be satisfied by choosing α in Eq. (3) sufficiently small. The overall adaptive algorithm is depicted in Fig. 3.

Conditions 3 and 4 are satisfied by any SPR filters H_1 and H_2 with nonredundant outputs (i.e., Rank $\{C_1\}$ = Rank $\{C_2\} = M$). For simplicity, they will be implemented in the experiment as the following first-order low-pass filters:

$$\dot{K}_I = -\sigma_1 K_I + L e_y \tilde{r}^T T \tag{17}$$

$$\dot{K}_p = -\sigma_2 K_p + \bar{L} e_y \tilde{r}^T \bar{T} \tag{18}$$

The branch filter F_B is implemented in the experiments as the first-order filter:

$$\dot{\tilde{e}}_y = (e_y - \tilde{e}_y)\gamma \tag{19}$$

For practical implementation, the preceding continuous-time adaptive control algorithm is discretized in time using a divided-difference approximation to the derivative.

V. Emulated Rate Sensing

A Kalman filter (KF) is used to estimate the rate from position measurements. It is emphasized that this approach is used to emulate a rate sensor which is not available in hardware, but which the algorithm requires. Hence, rigorously, the KF is not considered part of the adaptive control algorithm. However, information for the design of the KF was actually based on the coarse system description provided by a finite element model and not, for example, based on accurate system identification results. Hence, there is some indication that this approach may be useful for adaptive control of structures not having rate sensors.

Since the plant is specified in continuous time and the rate estimator is to be implemented in discrete time, there are essentially two ways to design it:

Table 1 Normal modes of vibration

Boom-dish modes			
	Frequency, Hz		
Mode no.	Axis 4–10 subsystem	Axis 1–7 subsystem	k
1	0.091	0.091	1
2	0.616	0.628	1
3	1.685	1.687	1
4	2.577	2.682	1
5	4.858	4.897	1
6	9.822	9.892	1
	Dish modes		
Mode no.	Frequency, Hz		k
1	0.210		0
2	0.253[a]		2
3	0.290[a]		3
4	0.322[a]		4
5	0.344[a]		5
6	0.351		6
7	1.517		0
8	1.533[a]		2
9	1.550[a]		3
10	1.566[a]		4
11	1.578[a]		5
12	1.583		6
13	4.656		0
14	4.658[a]		2
15	4.660[a]		3
16	4.661[a]		4
17	4.662[a]		5
18	4.663		6
19	9.474		0
20	9.474[a]		2
21	9.474[a]		3
22	9.474[a]		4
23	9.474[a]		5
24	9.474		6

[a]Two-fold degenerate modes.

1) Design a continuous-time Kalman filter and then discretize it.

2) Discretize the plant first and then design a discrete-time Kalman filter directly.

For plants with a full A_p matrix, approach 1 requires less computation since the state and measurement updates of the Kalman filter implementation are combined into a single equation. However, when the A_p matrix is block 2×2 diagonal as in the case of modal systems, approach 2 is much more efficient. This is because the 2×2 block structure is preserved by discretization of the A_p matrix directly, in contrast to approach 1 which destroys the 2×2 block structure by discretization of the (generally nonsparse) estimator matrix $(A_p - KC_p)$. Because of the severe computation time constraints imposed by the facility micro-Vax for real-time control implementation, computational efficiency was of prime importance, and method 2 was required. This is in contrast to earlier studies in Ref. 1 where smaller dimensional plants were used and method 1 was adequate.

Following method 2, the plant [(1) and (2)] is discretized exactly using a sampling period τ and assuming a zero-order hold on the inputs to give

$$x_{k+1} = \Phi x_k + \Gamma u_k + w_k \tag{20}$$

$$y_{k+1} = C_p x_k + v_k \tag{21}$$

where

$$\Phi = \exp(A_p \tau) \tag{22}$$

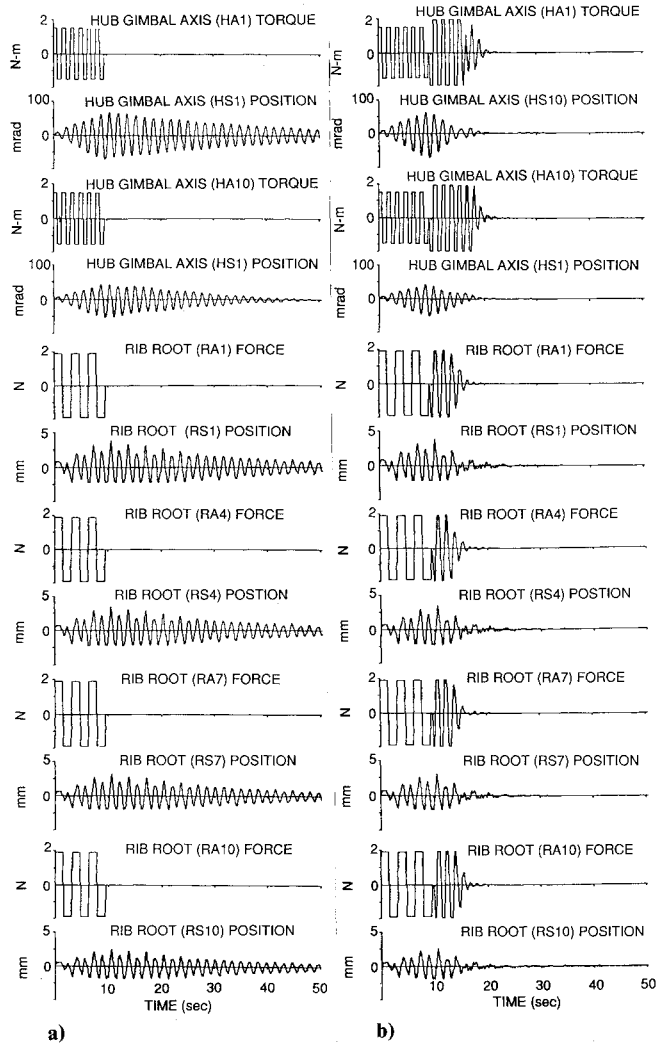

Fig. 4 Response to excitation involving 0.62-Hz pulse train through hub actuators and 0.32-Hz pulse train through rib root actuators: a) open-loop response; and b) closed-loop response.

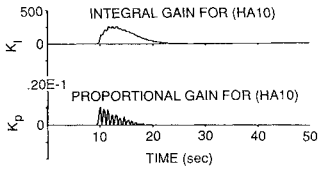

Fig. 5 Integral and proportional gains (HA10 axis).

$$\Gamma = \int_0^\tau \exp(A_p t) B_p \, dt \tag{23}$$

In Eqs. (20) and (21), we have modeled a system noise w and a sensor noise v to aid in the Kalman filter design. Note that the block 2×2 structure of A_p is preserved in Φ. The Kalman filter is designed based on the discretized system [(20) and (21)] and is implemented as the following two equations:

$$x_k(-) = \Phi x_{k-1}(+) + \Gamma u_{k-1} \tag{24}$$

$$x_k(+) = x_k(-) + K[y_k - C_p x_k(-)] \tag{25}$$

where the Kalman gain is determined by

$$K = PC_p^T [C_p P C_p^T + R]^{-1} \tag{26}$$

$$P = \Phi^T P \Phi - \Phi^T P C_p^T [C_p P C_p^T + R]^{-1} C_p P \Phi + Q \tag{27}$$

and

$$Q = E[w_k w_k^T], \qquad R = E[v_k v_k^T] \tag{28}$$

The noise covariances Q and R are used as tuning parameters for the filter design. It was found that the rate estimate was less sensitive to position bias when the choice of R is larger or equal to the choice of Q. To reflect the physical nature of system noise which enters as unknown torques on the system, and to reflect the uncertainty in the plant model used in the estimator design, covariance Q is chosen for the following form:

$$Q = \Gamma U \Gamma^T + \epsilon I$$

where

$$U = \nu \nu^T$$

and each component of vector ν is defined to be a small percentage of the typical signal level of a corresponding actuator.

A total of 24 modes were used in the estimator design, made up of the first four boom-dish modes on each orthogonal axis ($4 \times 2 = 8$ modes) plus the first 20 dish modes (note the two-fold degeneracies) minus four modes that were not observable or controllable from the chosen instrumentation. Accordingly, the highest boom-dish mode retained in the estimator design is 2.577 Hz, whereas the highest dish mode retained is 1.583 Hz. This places a fundamental restriction on the bandwidth over which the rate estimates remain accurate.

VI. Experimental Results

Because of the large number of signals to display in a multivariable application, the discussion here will focus on a single representative run. For this run the following choices are made for the adaptive control weightings and parameters: $L = \bar{L} = 5I$; $T = 10^4 I$; $\bar{T} = 6I$; $\sigma_1 = 0.5$ (0.08-Hz integral gain bandwidth); $\sigma_2 = 21.99$ (3.5-Hz proportional gain bandwidth); $\gamma = 37.7$ (6-Hz branch filter bandwidth); $\alpha = 0.0001$; and $\gamma = 0.045$ (sampling period).

The open-loop response to a simultaneous 0.62-Hz pulse train through the hub actuators and a 0.32-Hz pulse train through the rib root actuators is shown in Fig. 4a. As indicated in Table 1, this input simultaneously excites both the

boom-dish modes at 0.62 Hz, and the dish modes at 0.32 Hz. After the input excitation has stopped (9.6 s into the run), the structural response "rings" for about 73 s before dying out.

The closed-loop response to the same excitation is shown in Fig. 4b. Here the adaptive controller is turned on at 9.6 s into the run. It is seen that the closed-loop response settles out at about 11 s after the adaptive controller is turned on. It is seen that the settling time is reduced in closed-loop. Typical traces [(i.e., (HA10) location only] for the integral and proportional gains are shown in Fig. 5. It is seen that the integral gain builds in response to the output error and then decays with its assigned slow time constant $1/\sigma_1$. In contrast, the proportional gain tends to track the variations in output error due to its significantly faster time constant $1/\sigma_2$.

VII. Discussion

Several difficulties were encountered in the development phase of this task, which had to be overcome before successful operation was possible. A brief discussion is given here. Practical constraints on the experimental setup were mainly imposed by 1) limited computational capabilities of the DEC VAX station II workstation, and 2) the lack of rate measurements.

Unfortunately, these two problems enhance each other since reconstruction of the rates by Kalman estimation is computationally intensive.

In the present configuration, the multivariable adaptive controller requires the real-time tuning of 72 control gains for the regulation problem. Although somewhat formidable, the control computation was within the real-time capability of the VAX (utilizing optimized Fortran code and a sampling period of 45 ms). However, the lack of rate sensors requires the additional propagation of a 24-mode Kalman filter. At a sampling rate of 45 ms, the latter computational load stressed the timing loop beyond its capability and forced consideration of the following alternative approaches:

1) Discard the Kalman filter and use divided difference or other simple (model independent) approximations to the derivative of the position measurements.

2) Implement the Kalman filter at a lower sampling rate.

Neither of these approaches proved successful. Numerical approximations to the derivative (i.e., a "smoothed" derivative) induced lags in the control loop which invariably caused instability. On the other hand, lags induced from increasing the sampling period degraded performance substantially (the adaptive algorithm is derived in continuous time but is discretized by a divided-difference approximation). The problem was finally overcome using the method discussed in Sec. V, which retains the 2×2 block structure of the system in the estimator design. This latter approach reduced computation significantly, which allowed the return to a 45-ms sampling period.

Because of a nonideal plant, some tuning of the adaptive gain weightings and filter bandwidths was necessary to assure stable closed-loop performance. One major problem was due to actuator saturation. The resulting bang-bang effect caused high-frequency components which tended to excite a 4.6-Hz dish mode. Unfortunately, the present Kalman filter retains modes only up to 2.5 Hz and cannot accurately estimate rate at this frequency. This often resulted in instability, which could only be overcome by reducing adaptive gains and branch filter bandwidths accordingly.

Presently, a "human in the loop" tuning of the adaptive gain weightings is required to optimize the adaptive performance. Results on adaptive transient analysis using averaging methods[8] and numerical/symbolic optimization of the transient response[9] will be considered in the future to automate this process.

VIII. Conclusions

This paper documents recent experimental results in multivariable adaptive control of large flexible structures using the JPL LSCL three-dimensional ground test structure. The six-input/six-output control configuration is an upgrade to an earlier two-input/two-output configuration and extends control authority to four new actuator/sensor pairs located on the ribs. At the time of this writing, this experiment appears to be the largest adaptive control system successfully implemented in practice.

Because of the additional complexities of the six-input/six-output configuration, special processing techniques were required for rate estimation. The 24-mode discrete-time Kalman filter originally designed for use with smaller experiments was redesigned to preserve the 2×2 block structure of the continuous-time system, leading to significant computational savings. The performance of the adaptive controller was adjusted by using a human operator to modify the adaptation gain weights and filter bandwidths. The practical limitation to performance came from the need to avoid input saturation interacting with dish modes outside the rate estimator bandwidth. Reducing adaptation gain weights and filter bandwidths countered these effects and led to reasonable performance. Ongoing and future investigations will focus on the tracking problem and more systematic methods for optimizing the adaptive response.

Acknowledgments

The research described in this paper was carried out by the Jet Propulsion Laboratory, California Institute of Technology, under contract with NASA and the U.S. Air Force.

References

[1]Ih, C.-H. C., Bayard, D. S., Wang, S. J., and Eldred, D. B., "Adaptive Control Experiment with a Large Flexible Structure," *Proceedings of the AIAA Guidance, Navigation, and Control Conference* (Minneapolis, MN), AIAA, Washington, DC, Aug. 1988 (AIAA Paper 88-4153).

[2]Vivian, H. C. (ed.), *Flexible Structure Control Laboratory Development and Technology Demonstration,* Jet Propulsion Laboratory Publication 88-29, Pasadena, CA, Oct. 1987.

[3]Eldred, D. B., and Schaechter, D. B., "Hardware Verification of Distributed/Adaptive Control," *Proceedings of the Workshop on Applications of Distributed System Theory to the Control of Large Space Structures,* Jet Propulsion Laboratory Publication 83-46, Pasadena, CA, July 1983.

[4]Sundararajan, N., Montgomery, R. C., and Williams, J. P., "Adaptive Identification and Control of Structural Dynamics Systems Using Recursive Lattice Filter," NASA TP 2371, 1985.

[5]Sidman, D. S., "Adaptive Control of a Flexible Structure," Ph.D. Thesis, Stanford Univ., Stanford, CA, 1986.

[6]Rovner, D. M., and Franklin, G. F., "Experiments in Load-Adaptive Control of a Very Flexible One-link Manipulator," *Proceedings of the Fifth Yale Workshop on Applications of Adaptive Systems Theory,* Yale Univ., New Haven, CT, May 1987.

[7]Bayard, D. S., Ih, C.-H. C., and Wang, S. J., "Adaptive Control for Flexible Structures with Measurement Noise," *Proceedings of the American Control Conference* (Minneapolis, MN), June 1987, pp. 368–379.

[8]Bayard, D. S., "An Averaging Approach to Optimal Adaptive Control of Large Space Structures," *Proceedings of the American Control Conference* (San Diego, CA), May 1990, pp. 1576–1582; also in *Advances in Adaptive Control,* Selected Reprint Volume, edited by K. S. Narendra, R. Ortega, and P. Dorato, Inst. of Electrical and Electronics Engineers Press, New York, 1991.

[9]Peek, M.D., and Antsaklis, P. J., "Parameter Learning for Performance Adaptation," *IEEE Control Systems Magazine,* Vol. 10, No. 7, Dec. 1990, pp. 3–11.

[10]Sobel, K., Kaufman, H., and Mabius, L., "Implicit Adaptive Control Systems for a Class of Multi-Input Multi-Output Systems," *IEEE Transactions on Aero. Elect. Syst.,* Vol. AES-18, No. 5, 1982, pp. 576–590.